

# Plasma heating due to X-B mode conversion in a cylindrical ECR plasma system

Vipin K. Yadav<sup>†</sup> and D. Bora<sup>‡</sup>

*Institute for Plasma Research, Bhat, Gandhinagar, Gujarat - 382 428, India*

## Abstract

Extra Ordinary (X) mode conversion to Bernstein wave near Upper Hybrid Resonance (UHR) layer plays an important role in plasma heating through cyclotron resonance. Wave generation at UHR and parametric decay at high power has been observed during Electron Cyclotron Resonance (ECR) heating experiments in toroidal magnetic fusion devices. A small linear system with ECR and UHR layer within the system has been used to conduct experiments on X-B conversion and parametric decay process as a function of system parameters. Direct probing *in situ* is conducted and plasma heating is evidenced by soft x-ray emission measurement. Experiments are performed with hydrogen plasma produced with 160-800 W microwave power at 2.45 GHz of operating frequency at  $10^{-3}$  mbar pressure. The axial magnetic field required for ECR is such that the resonant surface ( $B = 875$  G) is situated at the geometrical axis of the plasma system. Experimental results will be presented in the paper.

## I. INTRODUCTION

Electron cyclotron resonance heating (ECRH) is a highly efficient, controllable and localized plasma heating [1] and current drive scheme in fusion machines such as tokamaks [2–5],

stellers [6] and plasma systems such as tandem mirrors [7]. These devices, when operated at high plasma densities (overdense plasma,  $\omega_{pe} > \omega_{ce}$ ), direct ECR heating and current drive by the incident electromagnetic (EM) wave is not possible. Alternatively, linear conversion of the EM waves into the electrostatic (ES) EBW [8] at the UHR surface and subsequent damping at the cyclotron harmonics is being tried for overdense plasmas [9].

In ECRH, the launched EM wave in extraordinary (X) mode, ( $\vec{k} \perp \vec{B}_0$  and  $\vec{E}_1 \perp \vec{B}_0$ ,  $\vec{k}$  is the wave vector,  $\vec{B}_0$  is the magnetic field in the system and  $\vec{E}_1$  is the wave electric field), is absorbed at the UHR surface in plasma as shown in the X-mode dispersion relation

$$\frac{c^2 k^2}{\omega^2} = 1 - \frac{\omega_{pe}^2}{\omega^2} \left( \frac{\omega^2 - \omega_{pe}^2}{\omega^2 - \omega_{uh}^2} \right) \quad (1)$$

where,  $\omega$  is the launched microwave frequency,  $\omega_{pe}$  is the electron plasma frequency and  $\omega_{uh}$  is the upper hybrid frequency given by

$$\omega_{uh}^2 = \omega_{pe}^2 + \omega_{ce}^2 \quad (2)$$

here,  $\omega_{ce}$  is the electron cyclotron frequency.

Near the UHR layer, the X-mode wavelength becomes very short and the amplitude of wave electric field becomes very large (high power-density). This large wave electric field gives rise to nonlinear phenomena of parametric excitation in which the incoming EM wave breaks up into EBW (X-B mode conversion) and lower hybrid (LH) wave [11]. The EBW propagates perpendicularly to the magnetic field towards the plasma centre and gets strongly damped at ECR layer as shown by the EBW dispersion relation given by

$$1 + \left( \frac{k_B v_{th}}{\omega_{pe}} \right)^2 = e^{(-k_B^2 r_L^2)} I_0(k_B^2 r_L^2) - 2 \left( \frac{\omega}{\omega_{ce}^2} \right) \sum_q e^{(-k_B^2 r_L^2)} \frac{I_q(k_B^2 r_L^2)}{\left( q^2 - \frac{\omega^2}{\omega_{ce}^2} \right)} \quad (3)$$

here,  $v_{th}$  is the electron thermal velocity,  $r_L$  is the electron Larmour Radius and  $I_q$  is the Bessel function of the first kind of imaginary argument,  $q = 1, 2, \dots$ . The absorption of EBW contribute in efficient plasma heating [12–14]

The parametric decay spectrum consists of wave with frequency of the incident pump wave,  $\omega$  and  $\omega \pm \omega_{LH}$ . The characteristic sidebands in the high-frequency spectrum and the associated

low-frequency waves from the parametric excitation have been observed in tokamaks [15] and stellarators [16,17].

The EBW is observed experimentally in linear or toroidal plasma system [18,13]. The EBW generation via mode conversion is observed in a large diameter linear plasma system with filament aided discharge [12].

## II. EXPERIMENTAL SET-UP

The experimental setup consists of a cylindrical stainless steel vacuum chamber with internal radius 6.4 cm and axial length 10 cm. A base pressure of  $6 \times 10^{-6}$  mbar is achieved prior to the experiment using a diffusion pump. The magnetic field is produced by two identical circular coils rested on the axial ports at the two ends of the vacuum vessel. Each magnetic field coil has an electrical resistance of  $30 \Omega$  and require 5.3 A of dc current to produce magnetic field of 875 G at the axis of the vacuum vessel which is kept constant for more than 1 second. The magnetic field contours in the system are shown in figure 2 [19].

The microwave system consists of a 800 W,  $2.45 \pm 0.02$  GHz magnetron, a three port circulator with water cooled dummy load to dissipate the reflected power, WR340 directional coupler, low barrier Schottky diode microwave detectors to measure forward and reflected power and a 10 mm thick,  $110 \text{ mm} \times 70 \text{ mm}$  rectangular toughen glass sheet to serve as the waveguide window. In absence of plasma  $\sim 80$  % of the forward power gets reflected whereas the reflected power drops to  $\sim 20$  % of the forward power in presence of plasma.

The plasma parameters are measured by a movable Langmuir probe [20] in the radial direction. The probe is made of tungsten with tip length and diameter of 5 mm and 0.5 mm respectively. A capacitive probe [21] as shown in figure 3, is used to measure the wave field. Probe signal is directly analysed with a spectrum analyser. Two capacitive probes [22] are used to measure the wave characteristics having tip length less than the expected wavelength to be detected, estimated theoretically as  $\approx 7.5$  mm. The signals from the capacitive probes are fed into two double balanced mixers (DBM). Each mixer has three ports : two input -

RF and LO (local oscillator) ports and one output - IF (intermediate frequency).

### III. EXPERIMENTAL RESULTS

ECR plasma is produced in the experimental system with hydrogen as the filling gas at an operating pressure of  $1 \times 10^{-3}$  mbar and an input microwave power of 800 W. The maximum plasma density,  $n_e$  in the system is  $3.1 \times 10^{10} \text{ cm}^{-3}$  at the geometrical axis of the system. Typical plasma temperature,  $n_e$  in the system is 12 eV. Radial profiles of  $f_{ce}$ ,  $f_{pe}$  and  $f_{uh}$  are calculated and plotted for the measured density and magnetic field profiles as shown in figure 4. Plasma density during the discharge for microwave power of 800 W is such that the UHR layer during the experiment lies at  $R = 2$  cm. The  $f_{uh}$  variation with input power is plotted in figure 5 which shows that despite the change in input power, the UHR layer position remains unchanged.

The parametric decay spectrum at UHR layer is shown in figure 7. The residual LH frequency is observed separately as shown in figure 8 which is calculated as 23.4 MHz hence, it matches well with the measured peaks. The capacitive probe is moved in hydrogen plasma from  $R = 0$  cm towards the UHR layer at  $R = 2$  cm. Figure 9 shows the capacitive probe output at the UHR layer as a function of microwave power that is increased gradually from 160 W to the maximum possible value of 800 W. As the power is increased, the spectrum is broadened on the lower frequency edge and at 300 W a peak starts appearing at 2.442 GHz which develops as the power is increased, Power threshold for excitation of the sideband is measured and the peak at 2.442 GHz appears only beyond 500 W of input power [21].

At the peak power, the signal is measured along the radius. As the capacitive probe is placed close to the UHR layer, within  $R = 1$  cm to  $R = 2$  cm, the original spectrum splits to smaller peaks as shown in figure 10. At UHR, the peak at  $f = 2.442$  GHz is distinct. The figure indicates the two ECR surfaces at  $R = 0$  and  $R = 6$  where the frequency spectrum is clean without fluctuations. The spectrum at  $R = 2$  (UHR surface) shows the side-peaks with the launched frequency indicating the parametric decay there. The frequency spectrum at

the radial positions near UHR surface,  $R = 1$  and  $R = 3$  contains fluctuations suggesting the splitting of power at UHR and propagation in both forward and reverse directions [21]. The EBW is detected and characterized with two identical capacitive probes [22]. The axial capacitive probe is fixed at  $R = 0$  cm and the radial capacitive probe is moved upto UHR layer. This small gap of 2 cm between the UHR and ECR layers limits the spatial resolution. The EBW parameters are given in the table below.

S.No.	Parameter	Value
1.	Gas	Hydrogen
2.	$f_0$ GHz	$2.45 \pm 0.02$
3.	$f_{EBW}$ GHz	2.438
4.	$\lambda_B$ mm	6.56
5.	$v_\phi$ $m s^{-1}$	$1.6 \times 10^7$
6.	$v_g$ $m s^{-1}$	$3.88 \times 10^4$
7.	$n_\perp$	20

The mode converted EBW propagate towards the centre of the experimental system near which the first ECR layer is residing. The EBW is absorbed at the ECR surface and gives rise to the localized electron heating. This is evident from the time evolution of plasma temperature as shown in figure 11 where the temperature increases with time and then attains a saturated value  $\approx 50$  eV afterwards for 800 W of input power. This indicates the absorption of the launched EM wave in the system. The localized heating of plasma with mode converted EBW in this experimental plasma system is further verified by the observation of the emission of soft x-rays [24].

The EEDF obtained from the Langmuir probe characteristics at the centre of the plasma chamber is shown in figure 12. Here,  $(V_p - V_B)$  is the accelerating voltage for the electrons in the plasma and  $dI/dV$  signifies the number of such electrons. In the figure, the hump in the tail of the distribution indicates the presence of high energy electrons with energies more than 100 eV. These energetic electrons hit metal targets of tungsten, molybdenum, etc. in

the plasma and leads to emission of soft x-ray. X-ray radiation from plasma can be energy resolved by using filters in the form of thin Aluminium foils.

In this experiment also the soft x-ray emission due to the generation of energetic electrons by the absorption of mode converted EBW is observed [24]. The soft x-ray emission signal with and without any target inside the plasma is shown in figure 13. This signal is very feeble compared to the one with Langmuir probe tip made of thoriated tungsten placed in the plasma. This indicates that the presence of a metal target increases the soft x-ray emission. The soft x-ray emission also depends on the nature of the metal target as shown in figure 14 where the signals for both the targets differ.

#### IV. CONCLUSION

Plasma heating due to X-B mode conversion is observed in a linear ECR plasma system. The X-B mode conversion is nonlinear in nature associated with parametric decay of the launched wave frequency. Parametric decay spectrum of the launched X-mode is observed at the UHR layer in system with capacitive probe. The decay spectrum contains  $\omega_0 \pm \omega_{LH}$  about the launched frequency,  $\omega_0$  (2.45 + 0.02 GHz) indicating the three-wave nonlinear interaction. The experimentally observed value of  $\omega_{LH}$  in the spectrum matches quite well with the estimated values. The parametric decay spectrum has an input power threshold ( $\approx 600$  W) to occur. This is in accordance with the estimated input power values. The parametric decay peaks are observed only near the calculated UHR layer in the system. The shift in probe position from UHR vanishes the peaks. The EBW generated near the UHR surface as a result of the mode conversion is experimentally observed and characterized. The EBW then propagates towards the first harmonic cyclotron resonance layer residing near the centre of the geometrical axis of the system and is absorbed. This absorption leads to the localized electron heating at that position. Experimental results indicate the presence of high energy electrons. This is further verified by EEDF obtained from the I-V characteristic at the centre of the system. The soft x-ray emission is observed from the ECR plasma using

a VPD. The soft x-ray signal is feeble in the absence of a target and gets enhanced in the presence of a tungsten target. The signal is also observed to be a dependent function of the material of the target.

## REFERENCES

<sup>†</sup> E-mail address: vipin@ipr.res.in

<sup>‡</sup> E-mail address: dbora@ipr.res.in

- [1] Brian Lloyd, Plasma Phys. Cont. Fusion, **40**, A119 (1998)
- [2] Wallace M. Manheimer, Infrared and Millimeter Waves Vol. 2 : Instrumentation, (Academic Press, New York, 1979), chapter 5, 299
- [3] A.C. England, IEEE Trans. Plasma Sci., **PS-12**, 124 (1984)
- [4] O.C. Eldridge and A.C. England, Nucl. Fusion, **29**, 1583 (1989)
- [5] V. Erckmann and U. Gasparino, Plasma Phys. Cont. Fusion, **36**, 1869 (1994)
- [6] V.V. Abrakov, D.K. Akulina, Eh. D. Andryukhina, *et. al.*, Nucl. Fusion, **37**, 233 (1997)
- [7] M. Porkolab, L. Friedland and I.B. Bernstein, Nucl. Fusion, **21**, 1463 (1981)
- [8] Ira B. Bernstein, Phys. Rev., **109**, 10 (1958)
- [9] A.D. Piliya, A. Yu Popov and E.N. Tregubova, Plasma Phys. Control. Fusion, **45**, 1309 (2003)
- [10] Thomas H. Stix, Phys. Rev. Lett., **15**, 878 (1965)
- [11] Ya. N. Istomin and T.B. Leyser, Phys. Plasmas, **2**, 2084 (1995)
- [12] H. Sugai, Phys. Rev. Lett., **47**, 1899 (1981)
- [13] S. Nakajima and H. Abe, Phys. Rev. A, **38**, 4373 (1988)
- [14] A.K. Ram and S.D. Schultz, Phys. Plasmas, **7**, 4084 (2000)
- [15] F.S. McDermott, G. Bekeffi, K.E. Hackett, J.S. Levine and M. Porkolab, Phys. Fluids, **25**, 1488 (1992)
- [16] H.P. Laqua, H. Maassberg, N.B. Marushchenko, F. Volpe, A. Weller, W7-AS Team, W.



- Kasperek and ECRH-Group, Phys. Rev. Lett., **90**, 075003-1 (2003)
- [17] H.P. Laqua, V. Erckmann, H.J. Hartfuß, H. Laqua, W7-AS Team and ECRH group, Phys. Rev. Lett., **78**, 3467 (1997)
- [18] W. Gekelman and R.L. Stenzel, Rev. Sci. Instrum., **46**, 1386 (1975)
- [19] Vipin K. Yadav and D. Bora, Pramana, **63**, 563, (2004)
- [20] I. Langmuir, Phys. Rev., **36**, 954 (1929)
- [21] Vipin K. Yadav and D. Bora, Phys. Plasmas, **11**, 3409 (2004)
- [22] Vipin K. Yadav and D. Bora, Phys. Plasmas, **11**, 4582 (2004)
- [23] C.V.S. Rao, Y. Shankara Joisa and C.J. Hansalia, A.K. Hui, Ratan Paul and Prabhat Ranjan, Rev. Sci. Instrum., **68**, 1142 (1997)
- [24] Vipin K. Yadav and D. Bora, Plasma Sources Sci. Technol., **13**, 231, (2004)

FIGURES

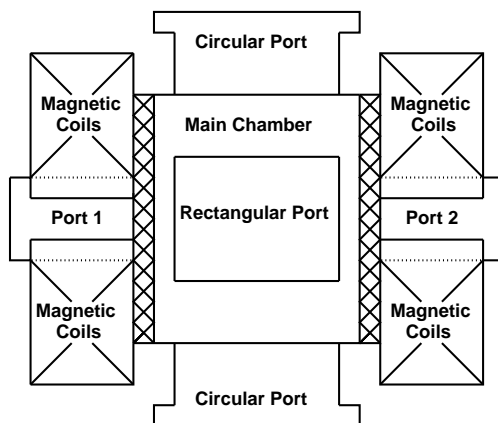


FIG. 1. Main chamber.

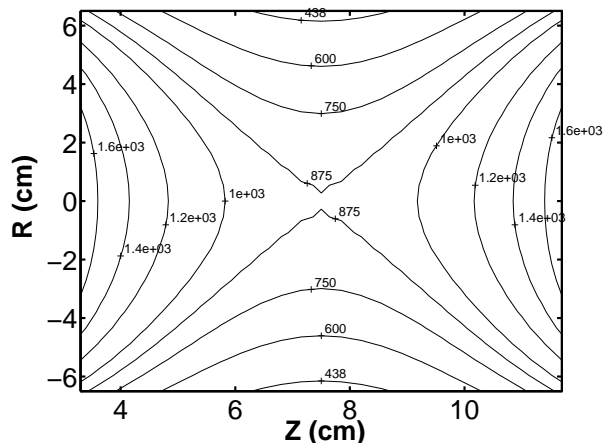


FIG. 2. Magnetic field contours in the system.

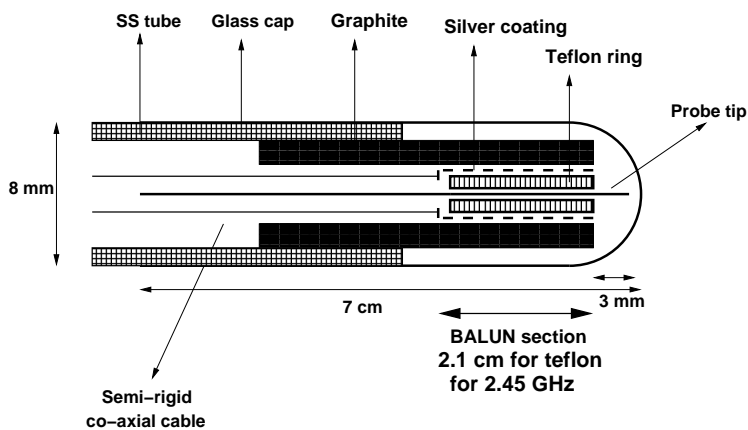


FIG. 3. Capacitive probe.

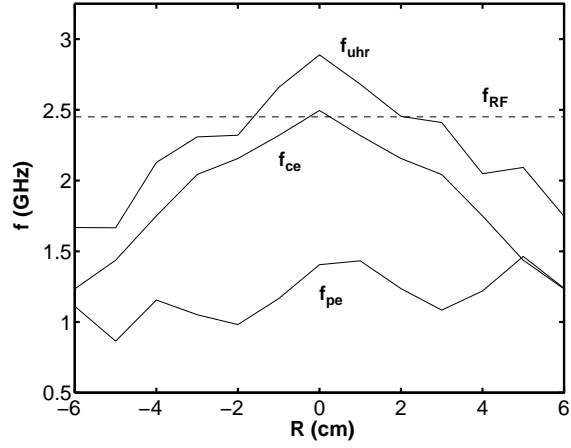


FIG. 4. Radial variation of  $f_{ce}$ ,  $f_{ce}$  and  $f_{uhr}$  in hydrogen plasma.

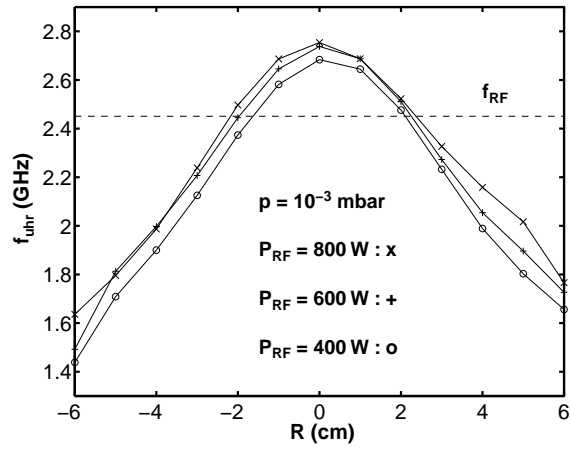


FIG. 5.  $f_{uhr}$  with input microwave power variation in hydrogen plasma.

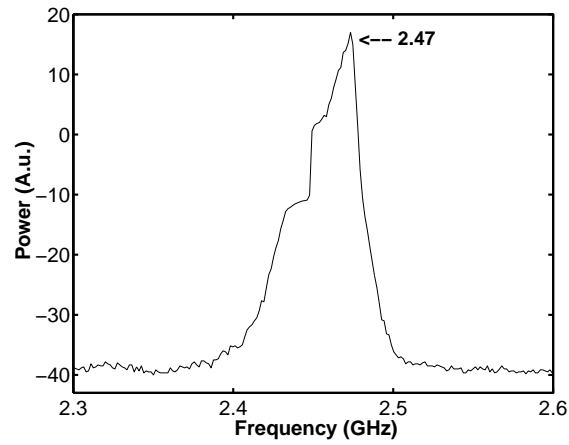


FIG. 6. Power output from magnetron at forward port of directional coupler.

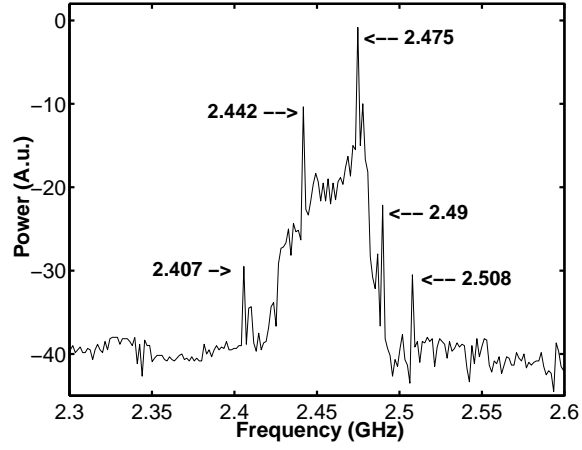


FIG. 7. Parametric decay spectrum in hydrogen plasma.

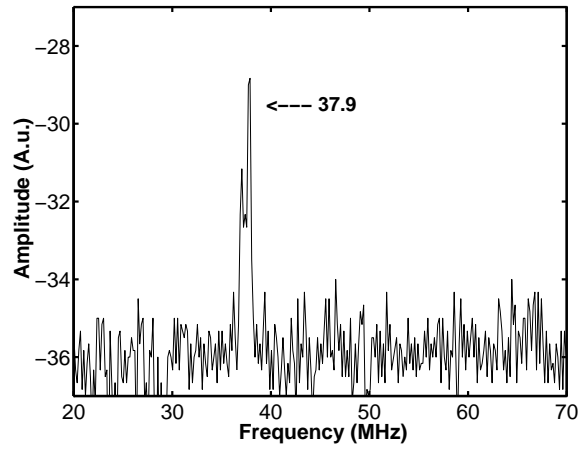


FIG. 8. The residual low frequency.

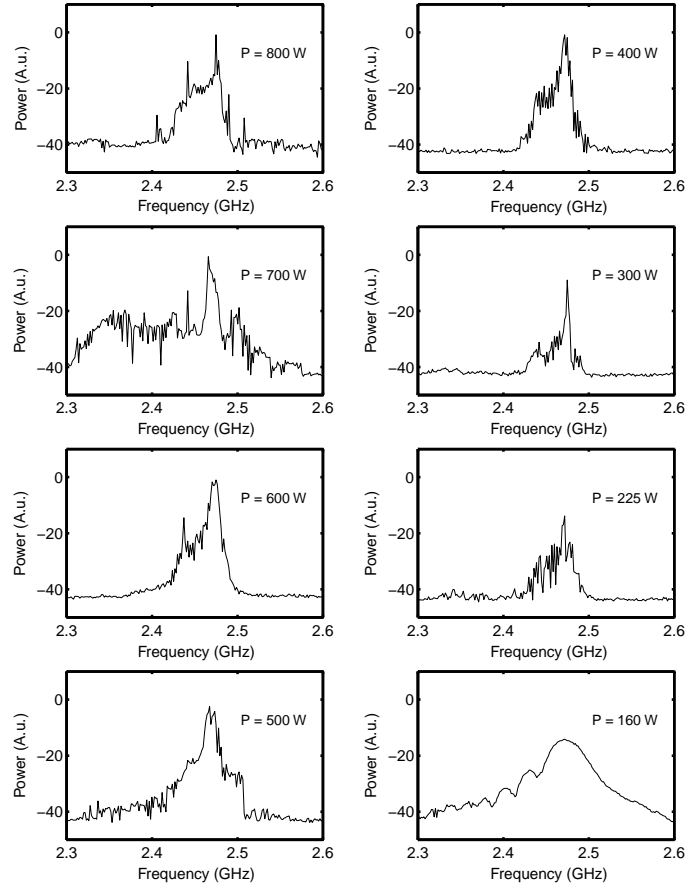


FIG. 9. Parametric decay spectrum with input microwave power variation.

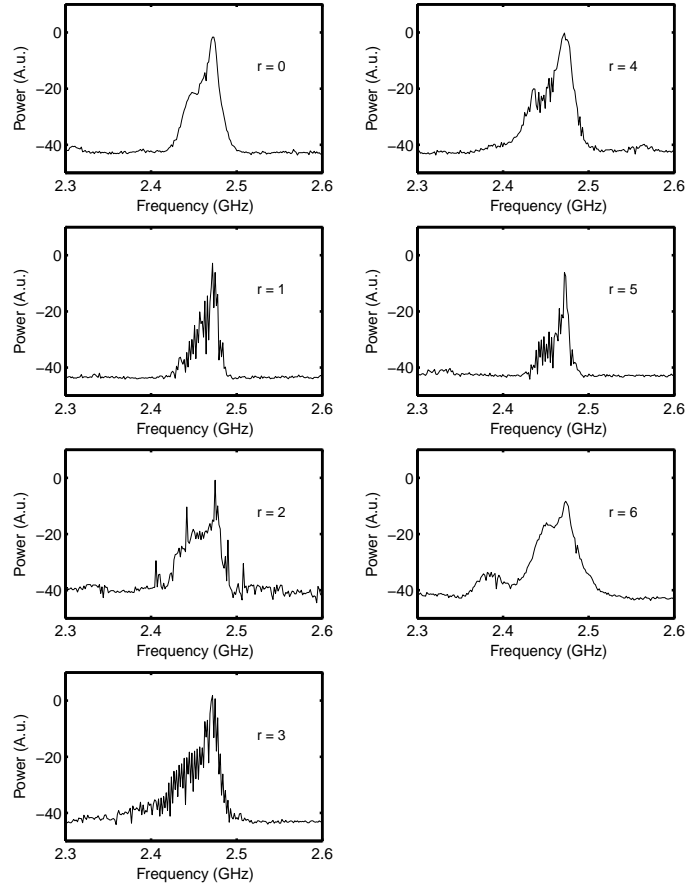


FIG. 10. Radial variation of parametric decay spectrum at 800 W input microwave power.

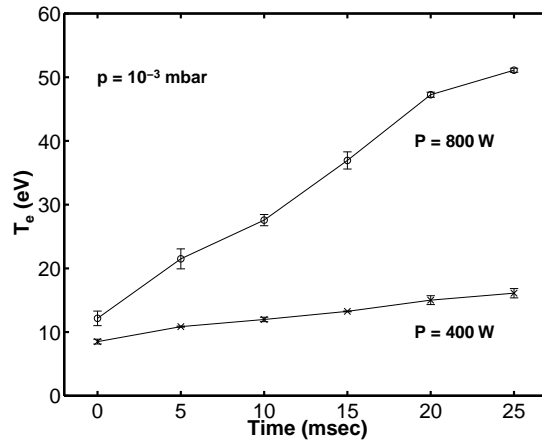


FIG. 11. Time evolution of plasma temperature in hydrogen plasma.

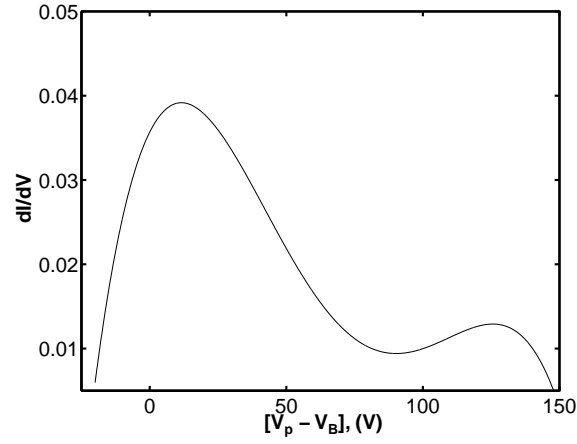


FIG. 12. The electron energy distribution function (EEDF).

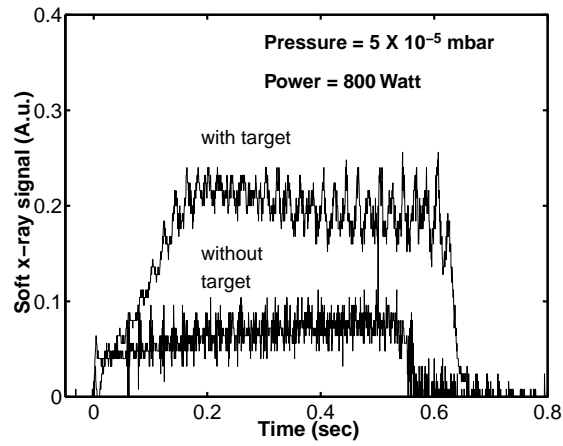


FIG. 13. Soft x-ray signal with and without metal target in plasma.

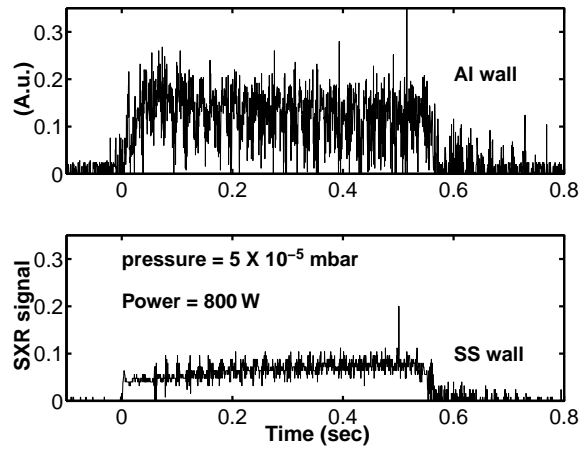


FIG. 14. Soft x-ray signal variation with Al and SS wall.